HHS Public Access

Author manuscript

Mol Cell Neurosci. Author manuscript; available in PMC 2019 January 21.

Published in final edited form as:

Mol Cell Neurosci. 2016 October ; 76: 21–32. doi:10.1016/j.mcn.2016.08.008.

KCa3.1 constitutes a pharmacological target for astrogliosis associated with Alzheimer's disease

Mengni Yi[#a], **Panpan Yu**[#b], **Qin Lu**[a], **Herbert M. Geller**[c], **Zhihua Yu**[a,*], and **Hongzhuan Chen**[a,*]

[a]Department of Pharmacology, Institute of Medical Sciences, Shanghai Jiao Tong University School of Medicine, Shanghai 200025, China

[b]Guangdong-Hongkong-Macau Institute of CNS Regeneration; Ministry of Education Joint International Research Laboratory of CNS Regeneration, Jinan University, Guangzhou 510632, China

[c]Developmental Neurobiology Section, Division of Intramural Research, National Heart, Lung, and Blood Institute, National Institutes of Health, Bethesda, MD 20892, USA

[#] These authors contributed equally to this work.

Abstract

Alzheimer's disease (AD) is the most common type of dementia and is characterized by a progression from decline of episodic memory to a global impairment of cognitive function. Astrogliosis is a hallmark feature of AD, and reactive gliosis has been considered as an important target for intervention in various neurological disorders. We previously found in astrocyte cultures that the expression of the intermediate conductance calcium-activated potassium channel KCa3.1 was increased in reactive astrocytes induced by TGF-β, while pharmacological blockade or genetic deletion of KCa3.1 attenuated astrogliosis. In this study, we sought to suppress reactive gliosis in the context of AD by inhibiting KCa3.1 and evaluate its effects on the cognitive impairment using murine animal models such as the senescence-accelerated mouse prone 8 (SAMP8) model that exhibits some AD-like symptoms. We found KCa3.1 expression was increased in reactive astrocytes as well as neurons in the brains of both SAMP8 mice and Alzheimer's disease patients. Blockade of KCa3.1 with the selective inhibitor TRAM-34 in SAMP8 mice resulted in a decrease in astrogliosis as well as microglia activation, and moreover an attenuation of memory deficits. Using KCa3.1 knockout mice, we further confirmed that deletion of KCa3.1 reduced the activation of astrocytes and microglia, and rescued the memory loss induced by intrahippocampal $A\beta_{1–42}$ peptide injection. We also found in astrocyte cultures that blockade of KCa3.1 or deletion of KCa3.1 suppressed Aβ oligomer-induced astrogliosis. Our

[*]Corresponding authors at: Department of Pharmacology, Institute of Medical Sciences, Shanghai Jiao Tong University School of Medicine, 280 South Chongqing Road, Shanghai 200025, China.

Disclosure statement

The authors disclose no actual or potential conflicts of interest. The protocol of animal experiments was approved by the Animal Experimentation Ethics Committee of Shanghai Jiao Tong University School of Medicine. All efforts were made to minimize the number of animals used and to minimize animal suffering. Human brain autopsy materials were collected from patients or donors from whom a written informed consent for a brain autopsy and the use of research tissue and clinical information after death had been obtained by the Netherlands Brain Bank.

Supplementary data to this article can be found online at http://dx.doi.org/10.1016/j.mcn.2016.08.008.

data suggest that KCa3.1 inhibition might represent a promising therapeutic strategy for AD treatment.

Keywords

Astrogliosis; Alzheimer's disease; GFAP; Mouse; Culture

1. Introduction

Alzheimer's disease (AD) is an age-related progressive neurodegenerative disease characterized by a gradual decline in cognitive function. It is the most common cause of dementia and is becoming increasingly prevalent in the aging population. AD is genetically divided in to familial cases and sporadic cases. Familial AD is a rare form that usually occurs with early onset (between age 30–60), and is caused by mutations in amyloid precursor protein (APP) or presenilins (Kahlfuss et al., 2014; Xia et al., 2015). In contrast, sporadic AD with a late onset after age 60 accounts for >90% of AD patients. The development of sporadic late-onset AD is more complex and is believed to be the result of a combination of genetic, environmental and lifestyle factors including age, vascular factors, inflammation, diabetes and susceptibility genes such as apolipoprotein E (APOE) (Piaceri et al., 2013). The neuropathological features of AD include the extracellular deposition of β-amyloid (Aβ) in senile plaques, intracellular neurofibrillary tangles (NFT) of hyperphosphorylated tau protein, neuropil threads, astrogliosis as well as microglia activation, eventually accompanied by neuronal loss and brain atrophy (Glass et al., 2010; Serrano-Pozo et al., 2011). The amyloid hypothesis, that aberrant accumulation of Aβ oligomers triggers a pathogenic cascade ultimately resulting in the development of AD, has been widely recognized and intensively investigated as a drug target for AD. However, recent failures of several amyloid-based drugs in clinical trials suggest that treatment for AD would require addressing multiple aspects in the pathogenesis of AD. Although Aβ toxicity and tau hyperphosphorylation have been considered as the two major causative pathophysiological mechanisms associated with the development of AD, emerging evidence implies that neuroinflammation and glial dysregulation may have a significant impact on the disease onset of AD (Aisen and Davis, 1994; Glass et al., 2010; Ralay Ranaivo et al., 2006; von Bernhardi, 2007; Yamazaki et al., 2014).

The intermediate-conductance Ca^{2+}-activated potassium channel KCa3.1, is involved in the activation and proliferation of many cell types including vascular smooth muscle cells, fibroblasts and inflammatory cells by regulating membrane potential and Ca^{2+} signaling (Di et al., 2010; Toyama et al., 2008; Yu et al., 2013a). In the central nervous system (CNS), several lines of evidence suggest that KCa3.1 is involved in the process of reactive astrogliosis that occurs in response to virtually all forms of CNS insults including trauma, stroke, infections and neurodegenerative disorders (Bouhy et al., 2011; Chen et al., 2011; Mauler et al., 2004). Serrano-Pozo et al. (2011) reported that KCa3.1 expression was increased in reactive astrocytes after spinal cord injury, while blockade of KCa3.1 with TRAM-34 improved neuronal survival and locomotor recovery. Blockade of KCa3.1 also decreased astrogliosis in glioblastomamultiforme-xenografted mice (D'Alessandro et al.,

2013). Mostly recently, using astrocyte cultures, we demonstrated that KCa3.1 plays an important role in astrogliosis induced by TGF-β and that genetic deficiency or pharmacological blockade of KCa3.1 with TRAM-34 attenuated the activation of astrocytes (Yu et al., 2014). Kaushal et al. (2007) reported that KCa3.1 was expressed in microglia in vitro, and that TRAM-34 could reduce microglial activation (Kaushal et al., 2007). Although reactive astrogliosis and microglia activation have long been recognized as pathological features of AD, the contribution of gliosis processes in the disease progression, especially in the early cognitive decline of AD is still poorly understood.

Based on the essential roles of KCa3.1 in activation of glial cells, found by us and others, in this study, we assessed the effect of KCa3.1 inhibition on the early cognitive impairment developed in the senescence-accelerated mouse prone 8 (SAMP8) mice, a spontaneous animal model of accelerated aging which develops early learning and memory deficits and other characteristics similar to those seen in AD patients, especially the most common sporadic form (Butterfield and Poon, 2005; Cheng et al., 2014; Miyamoto, 1997; Morley et al., 2012). We found that pharmacological blockade of KCa3.1 with TRAM-34 suppressed astrogliosis as well as microglia activation, and moreover attenuated early memory loss in SAMP8 mice. Using intrahippocampal injection of Aβ peptide to mimic AD, we further demonstrated that inhibition or genetic deletion of KCa3.1 had a beneficial role in ameliorating amyloid-induced ADlike symptoms.

2. Materials and methods

2.1. Animals

The SAMP8 mice and the senescence-accelerated mouse resistant R1 (SAMR1) mice were provided by the animal center of the First Affiliated Hospital of Tianjin University of Traditional Chinese Medicine. KCa3.1$^{-/-}$ mice were obtained from the Jackson Laboratory. The animals were housed in a specific pathogen-free animal facility with free access to food and water. The protocol of animal experiments was approved by the Animal Experimentation Ethics Committee of Shanghai Jiao Tong University School of Medicine.

2.2. Brain autopsy material

Paraffin-embedded human brain sections from six Alzheimer’s disease cases and six control cases were obtained from the Netherlands Brain Bank (Netherlands Institute for Neuroscience, Amsterdam). All material was collected from patients or donors from whom a written informed consent for a brain autopsy and the use of research tissue and clinical information after death had been obtained by the Netherlands Brain Bank.

2.3. Drug treatment

TRAM-34 (Apptec, WuXi, China) was prepared as previously described (Yu et al., 2013b). Briefly, TRAM-34 used for in vitro experiments was dissolved in dimethyl sulfoxide. For in vivo studies, TRAM-34 was dissolved in peanut oil. Seven-month-old male SAMP8 mice were treated with vehicle (peanut oil) or TRAM-34 (60 and 120 mg/kg, intraperitoneal) daily for 4 weeks. Age-matched male SAMR1 mice were used as normal controls. After 4 weeks of drug treatment, some of the mice were submitted to behavioral testing, while the

rest were euthanized and brain tissues were collected for real-time PCR, Western blotting or histology analyses.

2.4. *Preparation of $A\beta_{1-42}$ oligomer*

Oligomeric $A\beta_{1-42}$ was prepared as reported previously (Wang et al., 2012). Briefly, $A\beta_{1-42}$ (03–112, Life technologies) was initially dissolved in hexafluoroisopropanol (HFIP, Sigma, St. Louis, MO, USA) at 1 mg/ml and stored at −20 ˚C. For the aggregation of $A\beta_{1-42}$ oligomer, monomeric peptide dimethyl sulfoxide (DMSO) solution (5 mM) was diluted to 100 μM in Phosphate-buffered saline (PBS), pH 7.4, and incubated for 24 h at 4 ˚C.

2.5. *Stereotaxic intrahippocampal soluble $A\beta_{1-42}$ oligomers injection*

8–10 week old $KCa3.1^{+/+}$ and $KCa3.1^{-/-}$ male mice were anesthetized and injected bilaterally with 5 μl of soluble $A\beta_{1-42}$ oligomers (100 μM, 500 pmol/mouse) or PBS into the hippocampus at a rate of 1 μl/min. The stereotaxic coordinates used were as follows: 2.0 mm caudal to the bregma, 1.5 mm lateral from the midline, and 2.0 mm below the dural surface (Tang et al., 2014). Two weeks later, some of the mice were tested using the modified Morris water maze test, while the rest were perfused and the brain sections were prepared for immunostaining.

2.6. Morris water maze test

The modified Morris water maze test was carried out as described previously (Morris, 1984). The experimental apparatus consisted of a circular water tank (diameter = 80 cm; height = 50 cm) containing water at 22 ˚C, 25 cm deep and rendered opaque by adding an aqueous acrylic emulsion. A platform (diameter = 10 cm) was submerged 1 cm below the water surface and placed at the midpoint of 1 quadrant. The test involves 1-day of the visible platform test and 4-day of the hidden platform test, as well as a spatial probe trial. In brief, the latency was recorded as the time taken by the animal to find and climb onto the platform in the hidden platform test. The mice were allowed to swim freely for 60 s, were left for an additional 30 s period on the hidden platform, and were then returned to the home cage during the intertribal interval. In the spatial probe trial, each mouse was given two single probe tests without the platform and the percentage of total distance in target quadrant was measured. Mouse movement was recorded using a DigBehv-MM tracker system (Jiliang Software Technology Co., Ltd., Shanghai, China).

2.7. Real-time PCR

Quantitative analyses of mRNA levels of KCa3.1 in the brains of 7-month-old SAMR1 and SAMP8 mice were examined by real-time PCR. Briefly, cDNAs were prepared from total RNA using a RevertAid First Strand cDNA Synthesis kit (Fermentas). The Primer sequences were as follows: for KCa3.1, 5′-GGC TGA AAC ACC GGA AGCTC-3′ (Forward) and 5′-CAG CTC TGT CAG GGC ATCCA-3′ (Reverse); for β-actin, 5′-CAA CCG TGA AAA GAT GAC-3′ (Forward) and 5′- CAG GAT CTT CAT GAG GTAGT-3′ (Reverse). Real-time PCR was performed using SYBR Green (TaKaRa Biotechnology, Dalian, China) on an ABI 7500 sequencing system (Applied Biosystems). Steps used to perform qPCR analysis included a hold step at 50 ˚C for 2 min to activate uracil-DNA glycosylase, followed by

another hold at 95 ˚C for 10 min. Samples then underwent 40 cycles of 95 ˚C for 15 s followed by 60 ˚C for 1 min. Subsequently, melt analysis was performed by increasing the temperature from 65 to 95 ˚C. KCa3.1 gene expression levels were normalized using β-actin.

The final results, expressed as fold differences in target gene expression, relative to both endogenous control gene expression and the calibrator, were determined using the $2^{-\Delta\Delta CT}$ method.

2.8. Primary astrocyte cultures

Primary cortical astrocytes were prepared from neonatal (P0–P2) wildtype or KCa3.1$^{-/-}$ mouse brains as described previously (Wang et al., 2008). Briefly, the cerebral cortices were dissected out and dissociated into a single cell suspension. When astrocytes grew to confluence (10–14 days later), flasks were shaken overnight (200 rpm, 37 ˚C) to deplete microglia and oligodendrocyte precursor cells. The purified astrocytes were trypsinized and plated onto 12-mm glass coverslips (for Ca^{2+} imaging and immunocytochemistry), or six-well plates (for Western blotting) in serum-containing medium. After once again reaching confluence, astrocytes were serum-starved for 24 h and were then treated with 1 μM $A\beta_{1–42}$ oligomer for different time periods before harvest. In some cases, the cells were pre-treated with TRAM-34 1 h before addition of $A\beta_{1–42}$ oligomer.

2.9. Immunostaining and data analysis

12 μm thick brain sections were blocked with 3% bovine serum albumin (BSA) in PBS for 30 min at room temperature and were then incubated with the following primary antibodies: KCa3.1 (1:200, clone D-5, SantaCruz), GFAP (1:500, Z0334, Dako, Glostrup, Denmark), NeuN (1:100, ABN78, Millipore), Iba1 (1:500, 019–19741, Wako) at 4 ˚C overnight. Sections were washed three times with PBS and incubated with appropriate secondary antibodies: Alexa Fluor 488-conjugated or Alexa Fluor 568-conjugated anti-rabbit IgG (1:1000, Invitrogen); Alexa Fluor 488-conjugated or Alexa Fluor 568-conjugated anti-mouse IgG (1:1000, Invitrogen). Images were acquired using a Leica TCS SP8 Confocal Laser Scanning Microscope (Leica, Germany). For imaging acquisition, a prescan of all samples was performed to ensure confocal settings below saturation. For each experiment, all images were obtained using the same confocal settings. Six slices at 120 μm intervals from each brain were used to examine GFAP, Iba-1 and NeuN positive cells. Three microscopic fields (0.01 mm^2) were randomly selected in each slice with the same reference position for quantification. The GFAP, Iba-1 or NeuN positive cell number was counted in a blinded manner, and the area was measured by Leica LAS AF Lite software (Leica, Germany).

2.10. Western blot analysis

Cerebral cortices from the left hemisphere were homogenized in icecold lysis buffer [50 mM Tris, pH 7.4, 150 mM NaCl, 1 mM ethylenediaminetetraacetic acid (EDTA), 1% Triton X-100, 0.1% sodium dodecyl sulfate (SDS), supplemented with a protease inhibitor mixture (Sigma-Aldrich)] and were sonicated for 2 min. Cultured astrocytes were lysed with RIPA buffer [20 mM Tris-HCl, pH 8.1, 150 mM NaCl, 0.1% NP-40, 1% SDS, 0.5% sodium deoxycholate, 1 mM Phenylmethanesulfonyl fluoride (PMSF)]. The lysates were centrifuged

at 13,000 g for 10 min at 4 °C to remove insoluble materials. The protein concentration was determined using BCA assay. Equal amount of protein from each sample was subjected to SDS-polyacrylamide gel electrophoresis (10%) and was then transferred to polyvinylidenedifluoride (PVDF) membranes. Membranes were first incubated in blocking solution (5% nonfat dry milk in PBS with 0.05% Tween 20) for 1 h at room temperature and then incubated (overnight, 4 ˚C) with primary antibodies in the blocking solution. The following primary antibodies were used: anti-KCa3.1 (1:500; Alomone Labs), anti-GFAP (1:2000; Z0334, Dako), and anti-βactin (1:3000; Sigma). After rinsing with PBS containing 0.05% Tween 20, blots were incubated with HRP-conjugated anti-rabbit or antimouse antibody (1:3000; Amersham Biosciences) secondary antibodies in the blocking solution for 1 h at room temperature. Protein bands were identified using enhanced chemiluminescence reagents (Pierce, Rockford, IL). Images were captured on a Kodak Image Station; the immunoreactivity for each protein was quantified and was normalized to the corresponding β-actin loading control.

2.11. Calcium imaging

A confocal laser scanning microscope (Zeiss LSM 510 Meta; Carl Zeiss) was used to evaluate relative changes in intracellular calcium concentration ($[Ca^{2+}]_i$) by monitoring Fluo-4 fluorescence. Astrocyte cultures were loaded with 3 μM Fluo-4 AM (F-14,201; Invitrogen) for 30 min at 37 ˚C in an incubator, rinsed and incubated in DMEM with the appropriate pharmacological reagents. After a baseline recording, 5 μM Aβ oligomers were added to the cells at 30 s. TRAM-34 (10 μM) was added 1 h before the experiment. Fluo-4 fluorescence was measured at 510 nm with excitation at 488 nm. Confocal images were taken and stored every 2 s for 400 s. Data were obtained by evaluating the fluorescence from selected whole areas of cell bodies, and then taking the average of 10–20 cells.

2.12. Statistical analysis

All data are presented as Mean ± SEM. Statistical analyses were performed using Prism software (GraphPad Software, Inc., La Jolla, CA). Data were analyzed with Student’s t-test when comparing between two groups. One-way ANOVA and Dunnett’s post hoc tests were used for data with three or more groups. Statistical significance was set at $p < 0.05$.

3. Results

3.1. Up-regulation of KCa3.1 expression in the brains of SAMP8 mice and Alzheimer’s disease patients

We began by determining the expression of KCa3.1 in the brains of SAMP8 mice at 3-, 7- and 12- months of age. Age-matched SAMR1 mice were used as normal controls. We found a progressive upregulation of KCa3.1 protein in SAMP8 mice with age. Western blot results showed that the expression level of KCa3.1 was significantly increased in 7- and 12-month-old SAMP8 mice, compared to either 3-month-old SAMP8 mice, or to the age-matched SAMR1 mice (Fig. 1B, $p < 0.05$; n = 3 mice/group). Real-time PCR analysis also showed a significant elevation in KCa3.1 mRNA expression in SAMP8 mice at 7 months of age, compared to 7-month-old SAMR1 mice (Fig. 1C, $p < 0.01$; n = 4 mice/group).

To determine which cell types contributed to the increase of KCa3.1 expression, co-immunostaining of KCa3.1 with different cell-specific markers was performed on brain sections of 7-month-old SAMR1 and SAMP8 mice. The specificity of the KCa3.1 antibody was confirmed by staining brain sections of KCa3.1$^{-/-}$ mice; no obvious KCa3.1 staining was detected (Supplemental data). In SAMR1 mice, little expression of KCa3.1 was detected in GFAP^{+} astrocytes (Fig. 2A). However, in SAMP8 mice, where astrocytes in some brain regions became reactive, clear KCa3.1 expression was detected in some GFAP^{+} hypertrophic reactive astrocytes (Fig. 2A), which is consistent with previous reports in the injured spinal cord (Bouhy et al., 2011). Interestingly, in addition to the strong expression detected in reactive astrocytes, an upregulation of KCa3.1 was also found in some neurons. In SAMR1 mice, a weak KCa3.1 expression was found in NeuN^{+} neurons (Fig. 2B). However, much stronger KCa3.1 expression was detected in neurons of SAMP8 mice (Fig. 2B). Because it was reported that KCa3.1 is expressed in microglia in vitro (Bouhy et al., 2011; Kaushal et al., 2007), we also costained brain slices of SAMR1 and SAMP8 mice with KCa3.1 and the microglia marker Iba1. Rare co-localization was found between KCa3.1 and microglia in the brain slices of SAMP8 mice (Fig. 2C). Overall, these results demonstrated that, in control mice SAMR1, KCa3.1 was expressed at a low level mainly in neurons, while in SAMP8 mice, in addition to being up-regulated in neurons, KCa3.1 became expressed in reactive astrocytes and occasionally in microglia.

A similar up-regulation of KCa3.1 was observed in the brain sections of AD patients. KCa3.1 was only present at a low level in the NeuN^{+} neurons in the control human brain slices (Fig. 3B), while in AD patients, in addition to being up-regulated in neurons (Fig. 3B), KCa3.1 was expressed in GFAP^{+} reactive astrocytes (Fig. 3A), and rare colocalization was found between KCa3.1 and Iba1^{+} microglia (Fig. 3C).

3.2. KCa3.1 blockade rescues memory deficits in SAMP8 mice

Since KCa3.1 expression in SAMP8 mice was significantly increased with age, we next sought to test whether pharmacological blockade of KCa3.1 with TRAM-34 would exert beneficial effects on memory loss in SAMP8 mice. Seven-month-old SAMP8 mice and SAMR1 control mice were treated once daily with vehicle or TRAM-34 (60 and 120 mg/kg, intraperitoneal) for a total period of 4 weeks. The Morris water maze test was used to assess spatial learning and memory ability. Age matched SAMR1 mice were used as normal controls. In the hidden platform test, SAMP8 mice treated with vehicle showed deficits in their spatial learning and memory performance as compared with SAMR1 mice. In contrast, the group of SAMP8 mice treated with 120 mg/kg TRAM-34 exhibited significantly improved spatial learning and memory (Fig. 4A). No significant deficit was found in 3-month-old SAMP8 mice compared with SAMR1 mice (Fig. 4A). In the probe trial, after removing the escape platform, vehicle-treated SAMP8 mice swam significantly shorter time in the target quadrant than SAMR1 ($p < 0.01$, Fig. 4B). However, this was significantly improved in 120 mg/kg TRAM-34 treated SAMP8 mice ($p < 0.05$, Fig. 4B).

3.3. KCa3.1 blockade attenuates gliosis and neuronal loss in SAMP8 mice

Reactive astrogliosis and microglia activation are well-known pathological features of both the SAMP8 mouse and human AD (Verkhratsky et al., 2010). We and others have previous

shown in cell culture and a spinal cord injury animal model that inhibition of KCa3.1 can reduce the reactive glial response (Bouhy et al., 2011; Kaushal et al., 2007; Yu et al., 2014). To determine whether blockade of KCa3.1 with TRAM-34 also has an effect on gliosis in SAMP8 mice, GFAP and Iba-1 were used to detect reactive astrocytes and activated microglia, respectively. Both GFAP and Iba-1 immunoreactivity were significant increased in vehicle-treated SAMP8 mice as compared to the agematched SAMR1 mice. However, these glial responses were significantly suppressed by TRAM-34 treatment. A decrease of approximately 30% for $GFAP^+$ astrocytes (p b 0.01, Fig. 5A, B) and a decrease of approximately 50% for Iba-1^+ microglia ($p < 0.01$, Fig. 5C, D) were found in the group of 120 mg/kg TRAM-34 treated SAMP8 mice, compared with the vehicle-treated SAMP8 mice. In addition, TRAM-34 treatment also resulted in a reduction of neuronal loss. Compared with the vehicle-treated SAMP8 mice, significantly more $NeuN^+$ cells were found in the group of 120 mg/kg TRAM-34 treated SAMP8 mice ($p < 0.01$, Fig. 5E, F).

3.4. Genetic KCa3.1-deficiency reduces memory loss and gliosis induced by Aβ

Intrahippocampal administration of Aβ is one of the frequently used animal models to study AD by mimicking Aβ deposits, which can induce several AD-like phenotypes, including memory dysfunction (Borbely et al., 2014; Pearson-Leary and McNay, 2012). To provide additional evidence that KCa3.1 channels modulate the development of AD-like pathology and symptoms, we performed intrahippocampal injection of $Aβ_{1–42}$ oligomers in 8–10 week old wild type (WT, KCa3.$1^{+/+}$) and KCa3.1 knockout (KO, KCa3.$1^{-/-}$) mice. Mice received a single intrahippocampal injection of vehicle or Aβ oligomers (500 pmol/mouse). Two weeks later, spatial learning and memory were assessed using the Morris water maze test. During the 4-day training process, we found an obvious spatial learning deficit in WT mice that had received injections of Aβ oligomers, as exhibited by impaired performance in the Morris water maze test. However, KCa3.1 KO mice, to some degree, showed resistance to the Aβ-induced cognitive impairment and displayed better performance (Fig. 6A). After removing the escape platform, KCa3.1 KO mice injected with Aβ oligomers concentrated searches for the platform in the quadrant where it had been located, whereas WT mice injected with Aβ oligomers exhibited poorly focused search strategies (Fig. 6B). To assess the role of KCa3.1 in the gliosis and neuronal loss induced by Aβ oligomers, NeuN, Iba-1 and GFAP immunostaining was conducted in brain sections from vehicle- and Aβ-injected WT and KCa3.1 KO mice. Significantly fewer $GFAP^+$ astrocytes ($p < 0.01$; Fig. 7A, B) and $Iba1^+$ microglia ($p < 0.01$, Fig. 7C, D) were detected in the brains of KCa3.1 KO mice as compared to WT mice, while more $NeuN^+$ neurons were detected in the brains of KCa3.1 KO mice as compared to WT mice ($p < 0.05$; Fig. 7E, F). Overall, the behavior and histological findings obtained in KCa3.1 KO mice were consistent with those described after KCa3.1 blockade in the SAMP8 mice, supporting a role of KCa3.1 in the progression of cognitive impairment and pathological changes by regulating gliosis responses.

3.5. Involvement of KCa3.1 in Aβ oligomers induced reactive astrogliosis in vitro

To further study the potential role of KCa3.1 in the activation of astrocytes, we stimulated confluent cultures of astrocytes with $Aβ_{1–42}$ oligomers (1 μM) for 3 or 5 days. As shown in Fig. 8, exposure of astrocytes to $Aβ_{1–42}$ oligomers induced a time-dependent increase in KCa3.1 and GFAP protein expression ($p < 0.05$, Fig. 8A, B). To evaluate whether the up-

regulation of KCa3.1 contributes to the induction of reactive astrogliosis, cultured astrocytes were exposed to $A\beta_{1–42}$ oligomers (1 μM) in the presence or absence of TRAM-34 (1, 10 μM) for 3 days. Compared to control, astrocytes treated with $A\beta_{1–42}$ oligomers had a significant increase in GFAP expression ($p < 0.01$, Fig. 8C), while TRAM-34 significantly suppressed the effect of $A\beta_{1–42}$ oligomers on GFAP production ($p < 0.001$; Fig. 8C). This suggests that up-regulation of KCa3.1 in astrocytes occurs concomitantly with the process of reactive astrogliosis, and blockade of KCa3.1 inhibits astrocyte activation induced by the $A\beta_{1–42}$ oligomer. We also cultured astrocytes from KCa3.1$^{-/-}$ mice and evaluated their response to $A\beta_{1–42}$ oligomers. The absence of KCa3.1 in cultured astrocytes was confirmed by examining KCa3.1 protein expression using Western blotting (Fig. 8D). Similar to treatment of WT astrocytes with TRAM-34, astrocytes from KCa3.1$^{-/-}$ mice exhibited a decrease in GFAP expression in response to $A\beta_{1–42}$ oligomer treatment ($p < 0.01$, Fig. 8E) as compared to WT astrocytes, further indicating that KCa3.1 channels are involved in the reactive astrogliosis process.

3.6. *Blockade of KCa3.1 inhibited Aβ oligomer induced of Ca^{2+} influx in astrocytes*

Intracellular Ca^{2+} is thought to play a crucial role in almost all cellular processes, including regulation of reactive astrogliosis (Sofroniew and Vinters, 2010). Activation of KCa3.1 channels is thought to maintain a negative membrane potential which serves as a driving force for subsequent Ca^{2+} influx. We therefore sought to determine if the KCa3.1 channel is involved in Aβ oligomer-induced reactive astrogliosis by regulating Ca^{2+} flux. Astrocytes were loaded with the Ca^{2+} binding fluorescent dye Fluo-4 AM, and fluorescence was monitored in response to the application of Aβ oligomer. Application of 5 μM Aβ oligomer caused an acute increase in fluorescence intensity, with a maximum at 200 s after application; levels then declined such that $[Ca^{2+}]_i$ was at near control levels after 400 s. Aβ oligomer-induced increase in intracellular free Ca^{2+} in WT astrocytes was completely reversed by TRAM-34 (1 μM) (Figs. 9A, B). Moreover, there was no significant increase in intracellular free Ca^{2+} in astrocytes from KCa3.1$^{-/-}$ mice in response to $A\beta_{1–42}$ oligomer treatment (Fig. 9C, D). The above data suggest that the KCa3.1 channel plays an important role in Aβ oligomer-induced reactive astrogliosis by controlling intracellular Ca^{2+} entry.

4. Discussion

In this study, we found that expression of KCa3.1 was up-regulated in the brain of aged SAMP8 mice and AD patients, while pharmacological blockade of KCa3.1 with TRAM-34 significantly attenuated the astrogliosis and microglial activation that occurred in SAMP8 mice during aging. We also demonstrated that the gliosis response induced by intrahippocampal administration of Aβ was reduced after genetic deletion of KCa3.1. Taken together, these data provide evidence for a beneficial role of KCa3.1 inhibition in suppressing gliosis and preventing memory loss in AD.

The SAMP8 mouse model of accelerated aging is generally used in aging research. However, they also display several behavior and pathological features occurring in early AD, especially sporadic AD, which constitutes over 90% of all AD cases, so it has frequently been used as a model of AD (Butterfield and Poon, 2005; Cheng et al., 2014; Hansen et al.,

2015; Morley et al., 2012). Intrahippocampal administration of Aβ is also often used as a model of AD since it induces synaptotoxity and memory dysfunction, changes similar to those observed in AD (Borbely et al., 2014; Pearson-Leary and McNay, 2012). Even if these models cannot recapitulate all the aspects of AD, they are still useful for exploring potential therapeutic strategies for AD (Saraceno et al., 2013).

Astrogliosis has been considered as a promising therapeutic target in various CNS trauma and neurodegenerative disorders, including AD (Ralay Ranaivo et al., 2006; Schenk et al., 1999; Verkhratsky et al., 2010). The functions of normal astrocytes include providing essential metabolites to neurons, such as lactate, glutamine, and glutathione, which are reduced in reactive astrocytes of AD (Fuller et al., 2009). It appears that by transforming to a reactive phenotype, astrocytes redirect their efforts towards defensive and repair tasks at the expense of providing adequate metabolic support to neurons (Steele and Robinson, 2012). Astrogliosis and microgliosis were found abundantly around neuritic plaques and are involved in the inflammatory process of AD through the release of proinflammatory factors, cytokines, and reactive oxygen species (Heneka et al., 2001; Verkhratsky et al., 2010). Reactive astrocytes in AD model mice displayed elevated resting Ca^{2+} levels, more frequent Ca^{2+} transients and intracellular Ca^{2+} waves (Kuchibhotla et al., 2009). Activation of astrocytes by microglial inflammatory molecules combined with Ca^{2+} elevations may lead to abnormal gliotransmitter release including ATP, D-serine, glutamate and GABA, which contribute to synaptic damage, excitotoxicity, and neuro-degeneration in the diseased brain (Agulhon et al., 2012; Jo et al., 2014). All these suggest that modulating the gliotic response might be a potential target for AD.

The KCa3.1 channel was first detected in regard to volume regulation in human erythrocytes (Gardos, 1958). Voltage-independent KCa3.1 channels regulate Ca^{2+} influx by maintaining a negative membrane potential through K^+ efflux (Maylie et al., 2004). Evidence is accumulating that KCa3.1 plays important roles in diseases characterized by cell phenotype modulation, such as smooth muscle proliferation (Yu et al., 2013b), renal fibrosis (Huang et al., 2015), and astrogliosis (Yu et al., 2014). The anti-inflammatory and subsequently neuroprotective properties of KCa3.1 blockers have been shown in animal models of trauma, ischemic stroke, multiple sclerosis, spinal cord injury and optic nerve transactioninduced retinal ganglion degeneration (Maezawa et al., 2012; Wulff and Zhorov, 2008). Most recently, Chen et al. (2015) reported KCa3.1 expression in blood brain barrier endothelium in rat and human brain sections. Blockade of KCa3.1 significantly reduced Na^+ uptake and edema in the ischemic brain (Chen et al., 2015). However, the role of KCa3.1 in the progression of AD remains unknown. Because the characteristic of all these disorders involves neuroinflammation and gliosis, blockade of KCa3.1 is likely to improve the disease outcomes by attenuating the inflammatory situation and maintaining normal glial function. As KCa3.1 channels are responsible for maintaining a negative membrane potential to induce Ca^{2+} influx (Ferreira and Schlichter, 2013; Kahlfuss et al., 2014), inhibiting KCa3.1 channels is expected to return activated astrocytes to a quiescent phenotype and hence rescue the impaired neuronal function caused by a sustained gliosis response.

In this in vivo animal study, we found KCa3.1 was at low levels in the astrocytes of normal mice, but became up-regulated in the reactive astrocytes of SAMP8 mice and AD patients.

This was consistent with previous report in a model of spinal cord injury (Bouhy et al., 2011). It was reported that KCa3.1 channels are also expressed in microglia and macrophages in vitro and blockade of KCa3.1 channels attenuated several aspects of microglial activation such as migration, respiratory burst, and microglia-mediated neurotoxicity (Ferreira and Schlichter, 2013; Kaushal et al., 2007; Maezawa et al., 2011). Our results showed that KCa3.1 channels were expressed in microglia of both SAMP8 mice and AD patients, and that blockade or deletion of KCa3.1 reduced both astrogliosis as well as microgliosis in the mice. As we found KCa3.1 is also expressed in neurons, we cannot exclude the possibility that the beneficial role of KCa3.1 blockade observed in AD mice may be attributed partially to a direct effect on the neuronal KCa3.1 channels in addition to that of glial cells. However, the role of KCa3.1 in neurons needs further investigation.

Taken together, this study is the first to show in vivo age-dependent changes of the expression of KCa3.1, and the beneficial effects of KCa3.1 inhibition, on experimental models of AD. Our results revealed a role for the KCa3.1 channel in the development of AD-like symptoms and suggested that KCa3.1 may represent a novel promising therapeutic target for AD.

Supplementary Material

Refer to Web version on PubMed Central for supplementary material.

Acknowledgements

This work was supported by Science and Technology Commission of Shanghai Municipality grant 16ZR1418700, National Natural Science Foundation of China grant 81102491, Natural Science Foundation of Guangdong Province (2016A030313096), the Fundamental Research Funds for the Central Universities (21616340). The authors declare no competing financial interests.

References

Agulhon C, Sun MY, Murphy T, Myers T, Lauderdale K, Fiacco TA, 2012 Calcium signaling and gliotransmission in normal vs reactive astrocytes. Front. Pharmacol 3, 139. [PubMed: 22811669]

Aisen PS, Davis KL, 1994 Inflammatory mechanisms in Alzheimer's disease: implications for therapy. Am. J. Psychiatry 151, 1105–1113. [PubMed: 7518651]

Borbely E, Horvath J, Furdan S, Bozso Z, Penke B, Fulop L, 2014 Simultaneous changes of spatial memory and spine density after intrahippocampal administration of fibrillar abeta1–42 to the rat brain. Biomed. Res. Int 2014, 345305. [PubMed: 25050342]

Bouhy D, Ghasemlou N, Lively S, Redensek A, Rathore KI, Schlichter LC, David S, 2011 Inhibition of the Ca(2)(+)-dependent K(+) channel, KCNN4/KCa3.1, improves tissue protection and locomotor recovery after spinal cord injury. J. Neurosci 31, 16298–16308. [PubMed: 22072681]

Butterfield DA, Poon HF, 2005 The senescence-accelerated prone mouse (SAMP8): a model of age-related cognitive decline with relevance to alterations of the gene expression and protein abnormalities in Alzheimer's disease. Exp. Gerontol 40, 774–783. [PubMed: 16026957]

Chen YJ, Raman G, Bodendiek S, O'Donnell ME, Wulff H, 2011 The KCa3.1 blocker TRAM-34 reduces infarction and neurological deficit in a rat model of ischemia/reperfusion stroke. J. Cereb. Blood Flow Metab 31, 2363–2374. [PubMed: 21750563]

Chen YJ, Wallace BK, Yuen N, Jenkins DP, Wulff H, O'Donnell ME, 2015 Bloodbrain barrier KCa3.1 channels: evidence for a role in brain Na uptake and edema in ischemic stroke. Stroke 46, 237–244. [PubMed: 25477223]

Cheng XR, Zhou WX, Zhang YX, 2014 The behavioral, pathological and therapeutic features of the senescence-accelerated mouse prone 8 strain as an Alzheimer's disease animal model. Ageing Res. Rev 13, 13–37. [PubMed: 24269312]

D'Alessandro G, Catalano M, Sciaccaluga M, Chece G, Cipriani R, Rosito M, Grimaldi A, Lauro C, Cantore G, Santoro A, et al., 2013 KCa3.1 channels are involved in the infiltrative behavior of glioblastoma in vivo. Cell Death Dis 4, e773. [PubMed: 23949222]

Di L, Srivastava S, Zhdanova O, Ding Y, Li Z, Wulff H, Lafaille M, Skolnik EY, 2010 Inhibition of the K+ channel KCa3.1 ameliorates T cell-mediated colitis. Proc. Natl. Acad. Sci. U. S. A 107, 1541–1546. [PubMed: 20080610]

Ferreira R, Schlichter LC, 2013 Selective activation of KCa3.1 and CRAC channels by P2Y2 receptors promotes Ca(2+) signaling, store refilling and migration of rat microglial cells. PLoS One 8, e62345. [PubMed: 23620825]

Fuller S, Munch G, Steele M, 2009 Activated astrocytes: a therapeutic target in Alzheimer's disease? Expert. Rev. Neurother 9, 1585–1594. [PubMed: 19903019]

Gardos G, 1958 The function of calcium in the potassium permeability of human erythrocytes. Biochim. Biophys. Acta 30, 653–654. [PubMed: 13618284]

Glass CK, Saijo K, Winner B, Marchetto MC, Gage FH, 2010 Mechanisms underlying inflammation in neurodegeneration. Cell 140, 918–934. [PubMed: 20303880]

Hansen HH, Fabricius K, Barkholt P, Niehoff ML, Morley JE, Jelsing J, Pyke C, Knudsen LB, Farr SA, Vrang N, 2015 The GLP-1 receptor agonist liraglutide improves memory function and increases hippocampal CA1 neuronal numbers in a senescence-accelerated mouse model of Alzheimer's disease. J. Alzheimers Dis 46, 877–888. [PubMed: 25869785]

Heneka MT, Wiesinger H, Dumitrescu-Ozimek L, Riederer P, Feinstein DL, Klockgether T, 2001 Neuronal and glial coexpression of argininosuccinate synthetase and inducible nitric oxide synthase in Alzheimer disease. J. Neuropathol. Exp. Neurol 60, 906–916. [PubMed: 11556547]

Huang C, Pollock CA, Chen XM, 2015 KCa3.1: a new player in progressive kidney disease. Curr. Opin. Nephrol. Hypertens 24, 61–66. [PubMed: 25415613]

Jo S, Yarishkin O, Hwang YJ, Chun YE, Park M, Woo DH, Bae JY, Kim T, Lee J, Chun H, et al., 2014 GABA from reactive astrocytes impairs memory in mouse models of Alzheimer's disease. Nat. Med 20, 886–896. [PubMed: 24973918]

Kahlfuss S, Simma N, Mankiewicz J, Bose T, Lowinus T, Klein-Hessling S, Sprengel R, Schraven B, Heine M, Bommhardt U, 2014 Immunosuppression by N-methyl-Daspartate receptor antagonists is mediated through inhibition of Kv1.3 and KCa3.1 channels in T cells. Mol. Cell. Biol 34, 820–831. [PubMed: 24344200]

Kaushal V, Koeberle PD, Wang Y, Schlichter LC, 2007 The Ca2+-activated K+ channel KCNN4/KCa3.1 contributes to microglia activation and nitric oxide-dependent neurodegeneration. J. Neurosci 27, 234–244. [PubMed: 17202491]

Kuchibhotla KV, Lattarulo CR, Hyman BT, Bacskai BJ, 2009 Synchronous hyperactivity and intercellular calcium waves in astrocytes in Alzheimer mice. Science 323, 1211–1215. [PubMed: 19251629]

Maezawa I, Zimin PI, Wulff H, Jin LW, 2011 Amyloid-beta protein oligomer at low nanomolar concentrations activates microglia and induces microglial neurotoxicity. J. Biol. Chem 286, 3693–3706. [PubMed: 20971854]

Maezawa I, Jenkins DP, Jin BE, Wulff H, 2012 Microglial KCa3.1 channels as a potential therapeutic target for Alzheimer's disease. Int. J. Alzheimers Dis 2012, 868972. [PubMed: 22675649]

Mauler F, Hinz V, Horvath E, Schuhmacher J, Hofmann HA, Wirtz S, Hahn MG, Urbahns K, 2004 Selective intermediate-/small-conductance calcium-activated potassium channel (KCNN4) blockers are potent and effective therapeutics in experimental brain oedema and traumatic brain injury caused by acute subdural haematoma. Eur. J. Neurosci 20, 1761–1768. [PubMed: 15379997]

Maylie J, Bond CT, Herson PS, Lee WS, Adelman JP, 2004 Small conductance Ca2+activated K+ channels and calmodulin. J. Physiol 554, 255–261. [PubMed: 14500775]

Miyamoto M, 1997 Characteristics of age-related behavioral changes in senescence-accelerated mouse SAMP8 and SAMP10. Exp. Gerontol 32, 139–148. [PubMed: 9088911]

Morley JE, Armbrecht HJ, Farr SA, Kumar VB, 2012 The senescence accelerated mouse (SAMP8) as a model for oxidative stress and Alzheimer's disease. Biochim. Biophys. Acta 1822, 650–656. [PubMed: 22142563]

Morris R, 1984 Developments of a water-maze procedure for studying spatial learning in the rat. J. Neurosci. Methods 11, 47–60. [PubMed: 6471907]

Pearson-Leary J, McNay EC, 2012 Intrahippocampal administration of amyloid-beta(1–42) oligomers acutely impairs spatial working memory, insulin signaling, and hippocampal metabolism. J. Alzheimers Dis 30, 413–422. [PubMed: 22430529]

Piaceri I, Nacmias B, Sorbi S, 2013 Genetics of familial and sporadic Alzheimer's disease. Front. Biosci. (Elite Ed.) 5, 167–177. [PubMed: 23276979]

Ralay Ranaivo H, Craft JM, Hu W, Guo L, Wing LK, Van Eldik LJ, Watterson DM, 2006 Glia as a therapeutic target: selective suppression of human amyloid-betainduced upregulation of brain proinflammatory cytokine production attenuates neurodegeneration. J. Neurosci 26, 662–670. [PubMed: 16407564]

Saraceno C, Musardo S, Marcello E, Pelucchi S, Luca MD, 2013 Modeling Alzheimer's disease: from past to future. Front. Pharmacol 4, 77. [PubMed: 23801962]

Schenk D, Barbour R, Dunn W, Gordon G, Grajeda H, Guido T, Hu K, Huang J, Johnson-Wood K, Khan K, et al., 1999 Immunization with amyloid-beta attenuates Alzheimer-disease-like pathology in the PDAPP mouse. Nature 400, 173–177. [PubMed: 10408445]

Serrano-Pozo A, Frosch MP, Masliah E, Hyman BT, 2011 Neuropathological alterations in Alzheimer disease. Cold Spring Harb Perspect Med 1, a006189. [PubMed: 22229116]

Sofroniew MV, Vinters HV, 2010. Astrocytes: biology and pathology. Acta Neuropathol 119 (1), 7–35. 10.1007/s00401-009-0619-8 Epub 2009 Dec 10. Review. [PubMed: 20012068]

Steele ML, Robinson SR, 2012 Reactive astrocytes give neurons less support: implications for Alzheimer's disease. Neurobiol. Aging 33 (423), e1–13. [PubMed: 22244089]

Tang SS, Hong H, Chen L, Mei ZL, Ji MJ, Xiang GQ, Li N, Ji H, 2014 Involvement of cysteinyl leukotriene receptor 1 in Abeta1–42-induced neurotoxicity in vitro and in vivo. Neurobiol. Aging 35, 590–599. [PubMed: 24269024]

Toyama K, Wulff H, Chandy KG, Azam P, Raman G, Saito T, Fujiwara Y, Mattson DL, Das S, Melvin JE, et al., 2008 The intermediate-conductance calcium-activated potassium channel KCa3.1 contributes to atherogenesis in mice and humans. J. Clin. Invest 118, 3025–3037. [PubMed: 18688283]

Verkhratsky A, Olabarria M, Noristani HN, Yeh CY, Rodriguez JJ, 2010 Astrocytes in Alzheimer's disease. Neurotherapeutics 7, 399–412. [PubMed: 20880504]

von Bernhardi R, 2007 Glial cell dysregulation: a new perspective on Alzheimer disease. Neurotox. Res 12, 215–232. [PubMed: 18201950]

Wang H, Katagiri Y, McCann TE, Unsworth E, Goldsmith P, Yu ZX, Tan F, Santiago L, Mills EM, Wang Y, et al., 2008 Chondroitin-4-sulfation negatively regulates axonal guidance and growth. J. Cell Sci 121, 3083–3091. [PubMed: 18768934]

Wang Y, Xia Z, Xu JR, Wang YX, Hou LN, Qiu Y, Chen HZ, 2012 Alphamangostin, a polyphenolic xanthone derivative from mangosteen, attenuates beta-amyloid oligomers-induced neurotoxicity by inhibiting amyloid aggregation. Neuropharmacology 62, 871–881. [PubMed: 21958557]

Wulff H, Zhorov BS, 2008 K+ channel modulators for the treatment of neurological disorders and autoimmune diseases. Chem. Rev 108, 1744–1773. [PubMed: 18476673]

Xia D, Watanabe H, Wu B, Lee SH, Li Y, Tsvetkov E, Bolshakov VY, Shen J, Kelleher RJ, 3rd., 2015 Presenilin-1 knockin mice reveal loss-of-function mechanism for familial Alzheimer's disease. Neuron 85, 967–981. [PubMed: 25741723]

Yamazaki D, Horiuchi J, Ueno K, Ueno T, Saeki S, Matsuno M, Naganos S, Miyashita T, Hirano Y, Nishikawa H, et al., 2014 Glial dysfunction causes age-related memory impairment in Drosophila. Neuron 84, 753–763. [PubMed: 25447741]

Yu ZH, Wang YX, Song Y, Lu HZ, Hou LN, Cui YY, Chen HZ, 2013a Up-regulation of KCa3.1 promotes human airway smooth muscle cell phenotypic modulation. Pharmacol. Res 77, 30–38. [PubMed: 24055799]

Yu ZH, Xu JR, Wang YX, Xu GN, Xu ZP, Yang K, Wu DZ, Cui YY, Chen HZ, 2013b Targeted inhibition of KCa3.1 channel attenuates airway inflammation and remodeling in allergic asthma. Am. J. Respir. Cell Mol. Biol 48, 685–693. [PubMed: 23492185]

Yu Z, Yu P, Chen H, Geller HM, 2014 Targeted inhibition of KCa3.1 attenuates TGFbeta-induced reactive astrogliosis through the Smad2/3 signaling pathway. J. Neurochem 130, 41–49. [PubMed: 24606313]

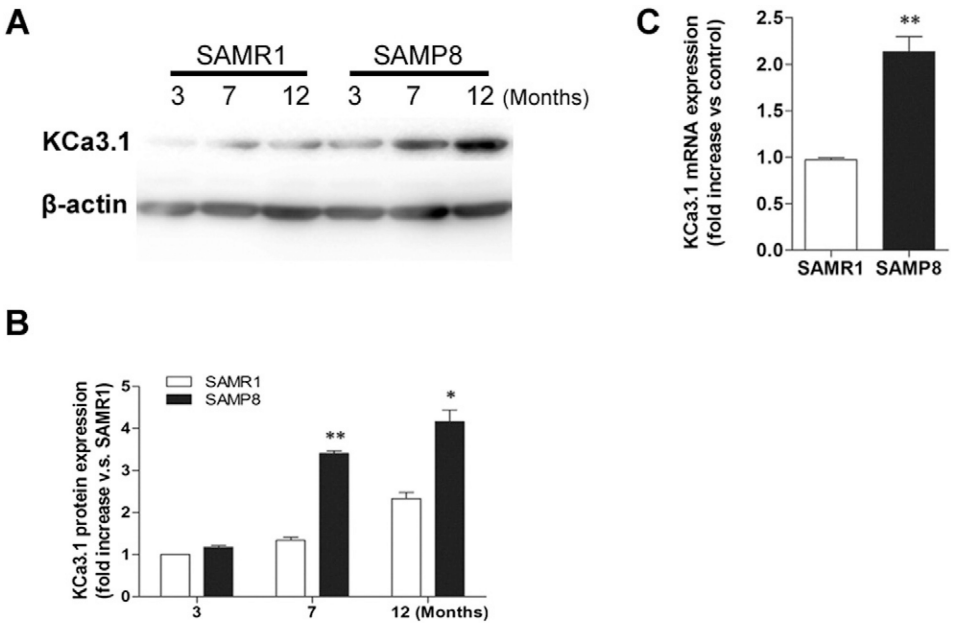

Fig. 1.

Up-regulation of KCa3.1 in the brains of SAMP8 mice. (A) Western blot analysis of KCa3.1 protein expression in the cortex of 3-, 7- and 12-month-old SAMR1 and SAMP8 mice. β-actin was used as the loading control. (B) The quantification of KCa3.1 protein expression in SAMR1 and SAMP8 mice (n = 3 each group). *$p < 0.05$, **$p < 0.01$, SAMP8 mice versus age-matched SAMR1 mice. (C) Quantitative real-time PCR analysis of KCa3.1 gene expression in 7-month-old SAMR1 and SAMP8 mice cortex. Values are shown for steady-state transcripts relative to β-actin in the same preparation. Results are expressed as mean ± SEM (n = 4). **$p < 0.01$, versus SAMR1 mice.

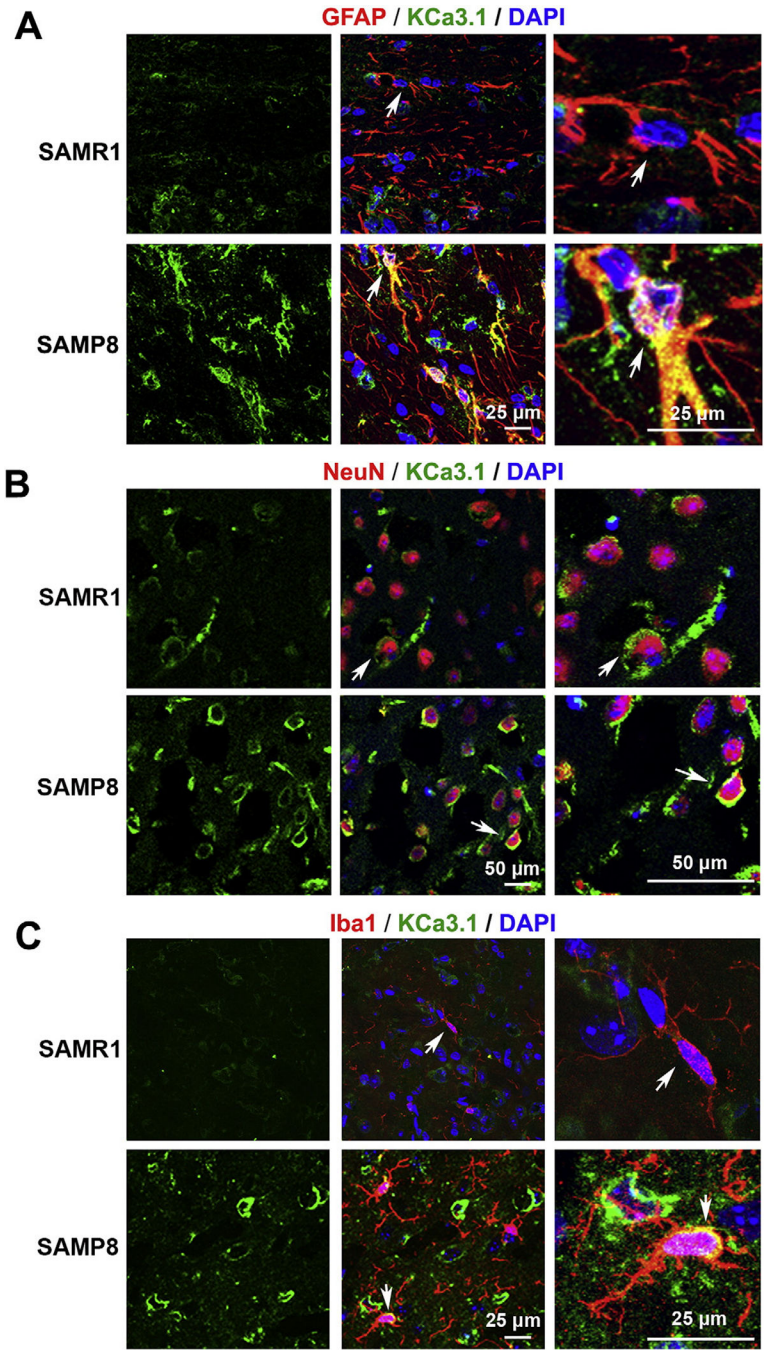

Fig. 2.

Up-regulation of KCa3.1 in reactive astrocytes and neurons of SAMP8 mouse brains. Double immunofluorescence staining of KCa3.1 (green) with GFAP (red), NeuN (red) or Iba1 (red) in brain sections of 7-month-old SAMR1 and SAMP8 mice. (A) Co-staining of KCa3.1 and GFAP in SAMR1 and SAMP8 mice; (B) Co-staining of KCa3.1 and NeuN in SAMR1 and SAMP8 mice; (C) Co-staining of KCa3.1 and Iba1 in SAMR1 and SAMP8 mice. Arrows indicate co-labeling of KCa3.1 and GFAP (A), KCa3.1 and NeuN (B) and KCa3.1 and Iba1 (C), views of which are enlarged in the adjacent panels. Nuclei were

stained in blue with DAPI. Scale bar: 25 μm in A; Scale bar: 50 μm in B; Scale bar: 25 μm in C.

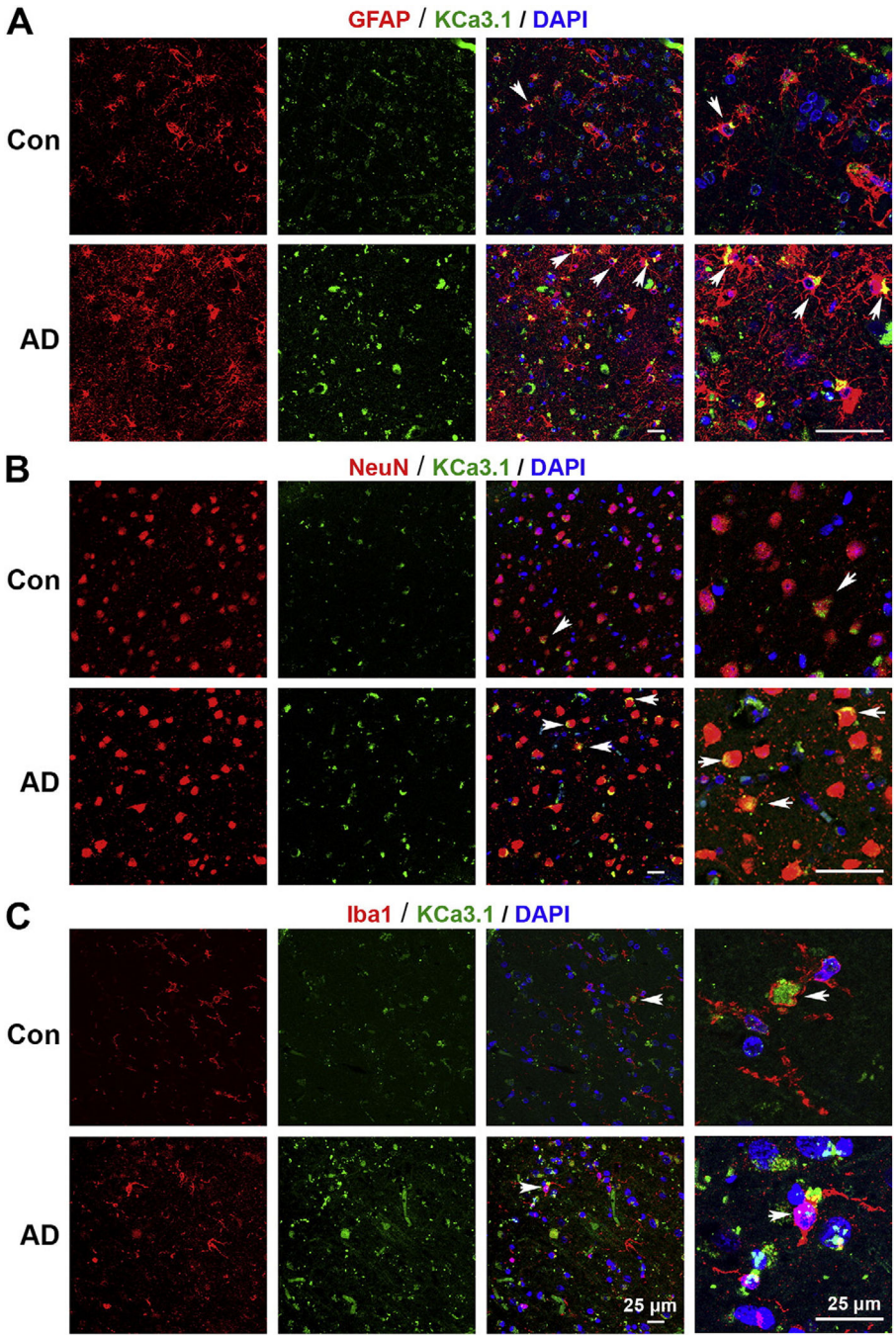

Fig. 3.

Up-regulation of KCa3.1 in reactive glial cells and neurons of Alzheimer's patient brains. Double immunofluorescence staining of KCa3.1 (green) with GFAP (red), NeuN (red) or Iba1 (red) in brain sections of control and AD patients. (A) Co-staining of KCa3.1 and GFAP in control human and AD patients; (B) Co-staining of KCa3.1 and NeuN in control human and AD patients; (C) Co-staining of KCa3.1 and Iba1 in control human and AD patients. Arrows indicate co-labeling of KCa3.1 and GFAP (A), the co-labeling of KCa3.1

and NeuN (B) and the co-labeling of KCa3.1 and Iba1 (C). Nuclei were stained in blue with DAPI. Scale bar: 25 μm.

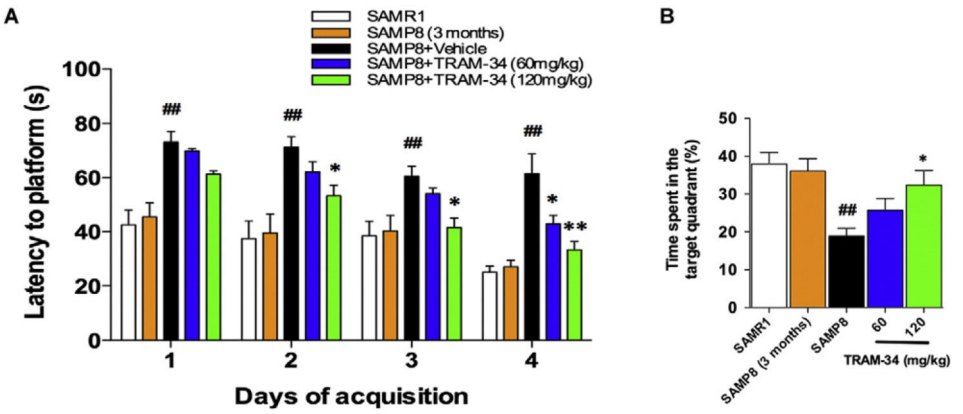

Fig. 4.

Blockade of KCa3.1 rescued memory deficits in SAMP8 mice using Morris water maze test. Seven-month-old SAMP8 mice (n = 8–10 per group) were treated with vehicle or TRAM-34 (60 or 120 mg/kg, intraperitoneal) daily for 4 weeks with the age-matched vehicle treated SAMR1 mice as normal controls, and three-month-old SAMP8 mice as negative controls. (A) Average daily escape latency; (B) Percentage of time spent in the target quadrant where the escape platform was located. Data represent mean ± SEM. $^{\#\#}p < 0.01$, versus SAMR1 mice. $^{*}p < 0.05$, $^{**}p < 0.01$, versus vehicle-treated SAMP8 mice.

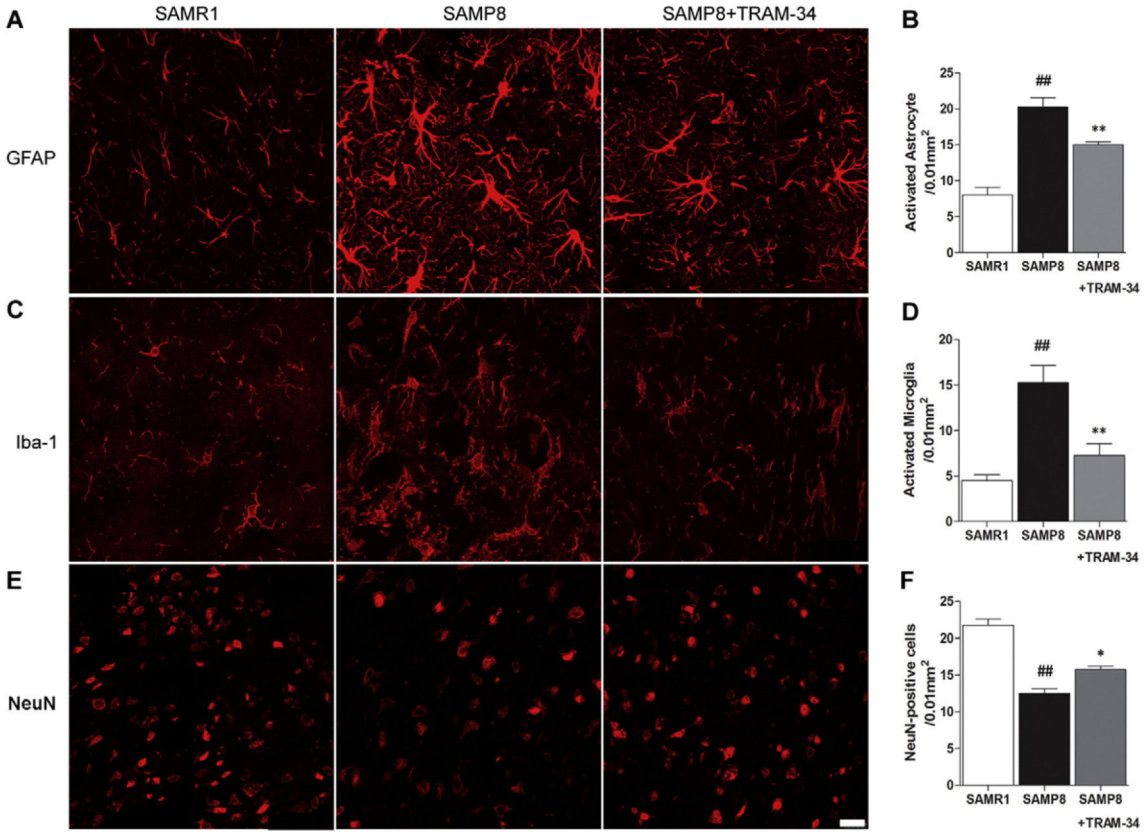

Fig. 5.

Blockade of KCa3.1 attenuated the activation of astrocytes and microglia in SAMP8 mice. Seven-month-old SAMP8 mice (n = 6–8 per group) were treated with vehicle or TRAM-34 (60 or 120 mg/kg, intraperitoneal) daily for 4 weeks with age-matched vehicle treated SAMR1 mice as normal controls. Brain sections were immunostained with anti-GFAP and anti-Iba-1 antibodies. (A) Representative images of GFAP-immunoreactive astrocytes from the hippocampal regions of SAMR1, SAMP8 or SAMP8 + TRAM-34 (120 mg/kg) groups. Scale bar: 50 μm. (B) Quantification of reactive astrocyte number/0.01 mm^2 in the hippocampus (n = 6–8). Data represent mean ± SEM. $^{\#\#}p < 0.01$, versus SAMR1 mice. $^{**}p < 0.01$, versus vehicle-treated SAMP8 mice. (C) Iba-1 immunoreactivity demonstrated active microglia from the hippocampal regions of SAMR1, SAMP8, and SAMP8 + TRAM-34 (120 mg/kg) groups. Scale bar: 25 μm. (D) Quantification of activated microglia number/0.01 mm^2 in the hippocampus (n = 6–8). (E) NeuN immunoreactivity demonstrated neurons in the hippocampal regions of SAMR1, SAMP8, and SAMP8 + TRAM-34 (120 mg/kg) groups. Scale bar: 25 μm. (F) Quantification of neuron number/0.01 mm^2 in the hippocampus (n = 6–8). Data represent mean ± SEM. $^{\#\#}p < 0.01$, versus SAMR1 mice. $^{**}p < 0.01$, versus vehicle-treated SAMP8 mice.

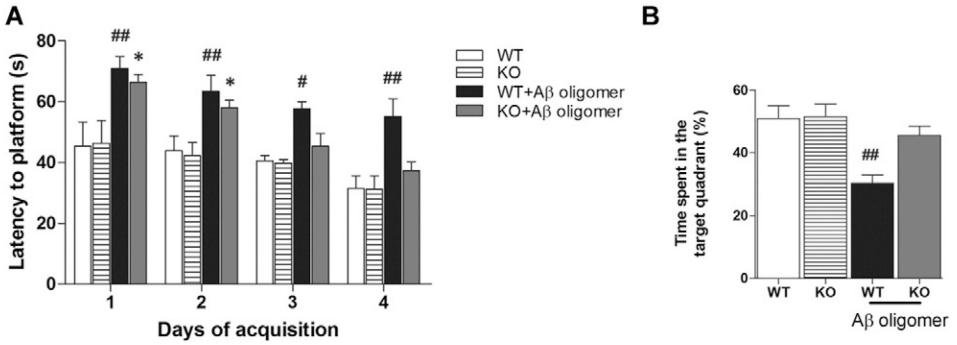

Fig. 6.

KCa3.1 deletion rescued memory deficits after hippocampal injection of Aβ oligomers. (A) Escape latency; (B) Percentage of time spent in the target quadrant where the escape platform had been located for groups of WT (n = 8–10) and KCa3.1$^{-/-}$ (n = 8–10) mice after intrahippocampal injection of Aβ oligomers. Data represent mean ± SEM. $^{\#}p < 0.05$, $^{\#\#}p < 0.01$, versus vehicle treated WT mice. $^{*}p < 0.05$ versus vehicle treated KCa3.1$^{-/-}$ mice. WT, wild type; KO, knockout.

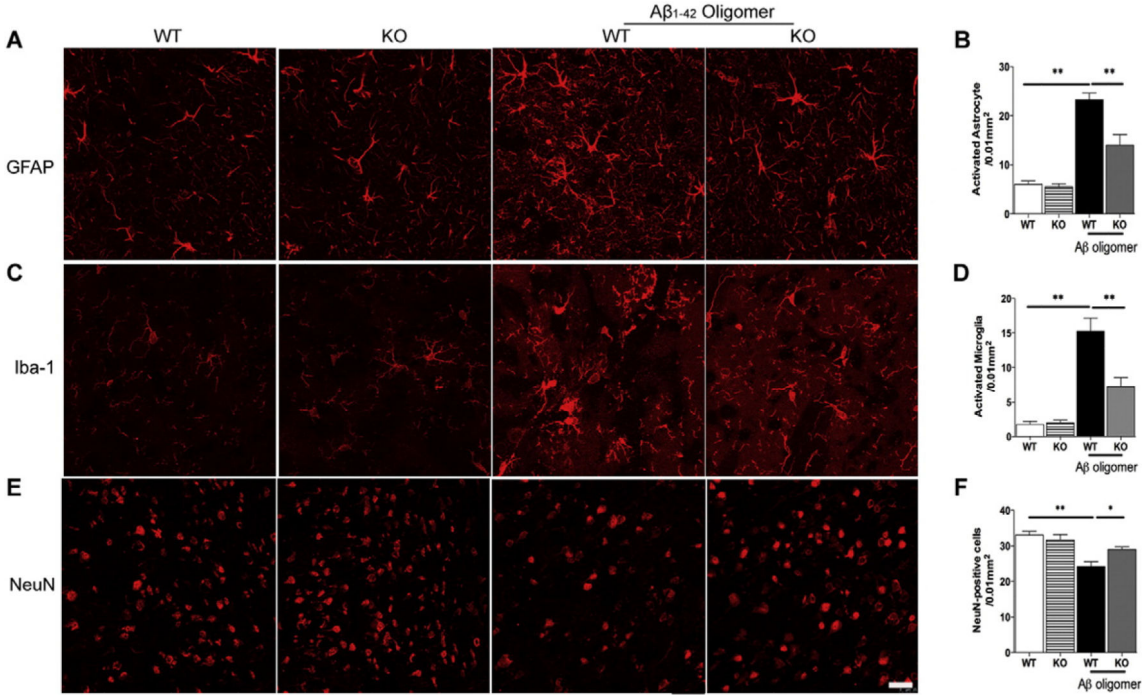

Fig. 7.

KCa3.1 deletion attenuated gliosis in response to hippocampal injection of Aβ oligomers. (A) Representative images of GFAP-immunoreactive astrocytes from the hippocampal regions of WT or KCa3.1 KO mice at 14 days after Aβ oligomer injection. Scale bar: 50 μm. (B) Quantification of reactive astrocyte number/0.01 mm^2 in the hippocampus (n = 6–8). (C) Iba-1 immunoreactivity demonstrated active microglia from the hippocampal regions of WT or KCa3.1 KO mice at 14 days after Aβ oligomer intrahippocampus injection. Scale bar: 25 μm. (D) Quantification of activated microglia number/0.01 mm^2 in the hippocampus (n = 6–8). (E) NeuN immunoreactivity demonstrated neurons from the hippocampal regions of WT or KCa3.1 KO mice at 14 days after Aβ oligomer injection. Scale bar: 25 μm. (F) Quantification of activated microglia number/0.01 mm^2 in the hippocampus (n = 6–8). Data represent mean ± SEM. $^{**}p < 0.01$, versus vehicle or Aβ oligomers injected WT mice (n = 6–8). WT, wild type; KO, knockout.

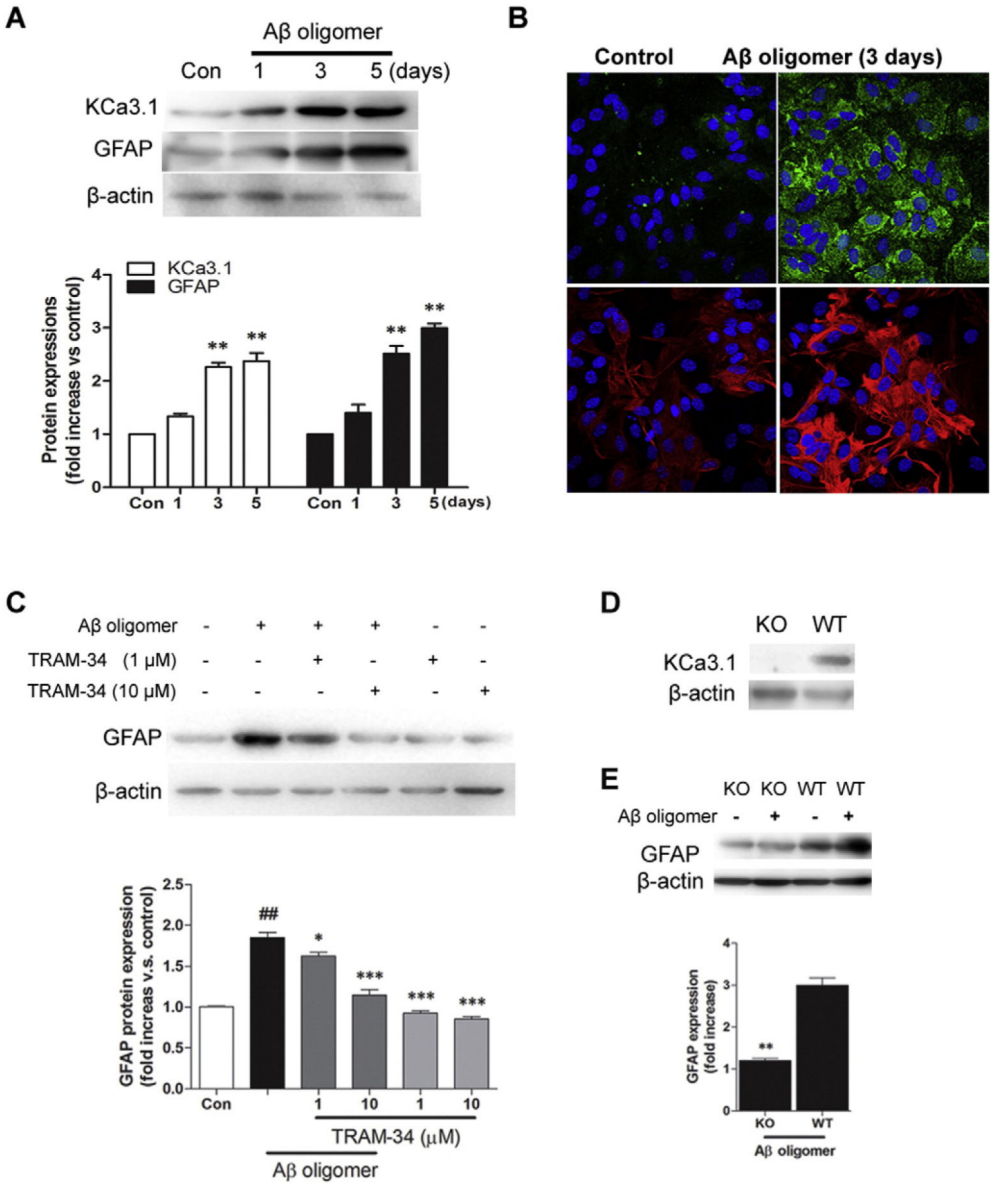

Fig. 8.

Involvement of KCa3.1 in Aβ oligomer induced reactive astrogliosis. (A) Representative western blot showing stimulation with 1 μM Aβ oligomer increased KCa3.1 and GFAP protein expression in cultured astrocytes in a time-dependent fashion. Quantification of western blot for KCa3.1 and GFAP expression in astrocytes after Aβ oligomer treatment (n = 3). Con: control. Data are presented as mean ± SEM. $*p < 0.05$ versus control. (B) Representative immunocytochemistry showing stimulation with 1 μM Aβ oligomer for 3 days increased KCa3.1 and GFAP protein expression in cultured astrocytes. (C) Representative western blot showing GFAP expression in cultured astrocytes treated with 1 μM Aβ oligomer for 3 days in the presence of TRAM-34 (1, 10 μM). Quantification of western blot for GFAP expression (n = 3). Con: control. Data are presented as mean ± SEM. $^{\#\#}p < 0.01$ versus control, $*p < 0.05$, $***p < 0.001$ versus Aβ oligomer alone. (D) Western blot showing the absence of KCa3.1 expression in the astrocytes of KCa3.1 KO mice. (E)

Representative western blot and quantification of GFAP expression after Aβ oligomer treatment in WT and KCa3.1 KO astrocytes (n = 3–4). $^{**}p < 0.01$ versus WT. WT, wild type; KO, knockout.

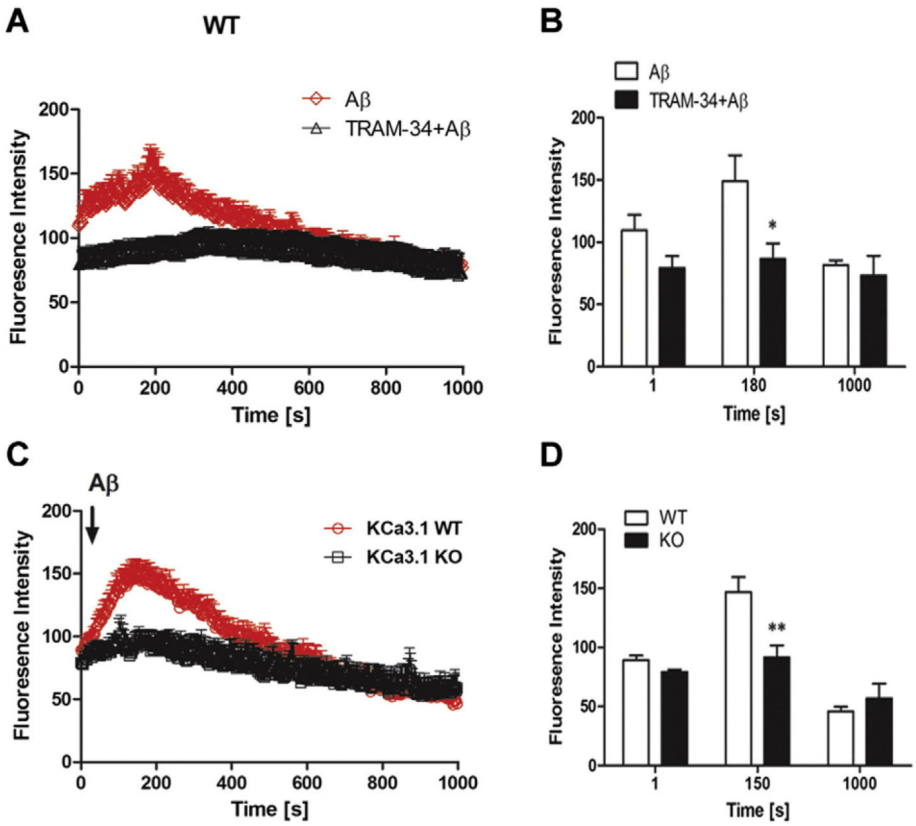

Fig. 9.

Involvement of KCa3.1 in Aβ oligomer-induced intracellular calcium increase in astrocytes. Astrocytes were loaded with the Ca^{2+}-sensitive dye Fluo-4 AM at 37 ˚C for 30 min and changes in $[Ca^{2+}]_i$ were monitored by confocal microscopy. 5 μM Aβ oligomer was added to astrocytes at 30 s with or without pre-treated TRAM-34 (1 μM) (A). Summary of data showing intracellular Ca^{2+} (B) at 1 s, 180 s (peak of fluorescence) and 1000 s. $*p < 0.05$ versus Aβ oligomer-stimulated cells.5 μM Aβ oligomer was added to WT and KCa3.1 KO astrocytes at 30 s (C). Summary of data showing intracellular Ca^{2+} (D) at 1 s, 150 s (peak of fluorescence) and 1000 s. Signal acquisition lasted for 1000 s. Data are presented as means ± SEM (n = 20 cells). $**p < 0.01$ versus WT cells. WT, wild type; KO, knockout.